Smart Structures and Systems, *Vol. 26, No. 5* (*2020*) *591-603*
DOI: https://doi.org/10.12989/sss.2020.26.5.591

Dynamic deflection monitoring of high-speed railway bridges with the optimal inclinometer sensor placement

Shunlong Li*[1], Xin Wang[1], Hongzhan Liu[2], Yi Zhuo[2], Wei Su[2] and Hao Di[2]

[1]*School of Transportation Science and Engineering, Harbin Institute of Technology, 73 Huanghe Road, 150090 Harbin, China*
[2]*China Railway Design Corporation, 300142 Tianjin, China*

(*Received December 25, 2019, Revised March 11, 2020, Accepted July 27, 2020*)

Abstract. Dynamic deflection monitoring is an essential and critical part of structural health monitoring for high-speed railway bridges. Two critical problems need to be addressed when using inclinometer sensors for such applications. These include constructing a general representation model of inclination-deflection and addressing the ill-posed inverse problem to obtain the accurate dynamic deflection. This paper provides a dynamic deflection monitoring method with the placement of optimal inclinometer sensors for high-speed railway bridges. The deflection shapes are reconstructed using the inclination-deflection transformation model based on the differential relationship between the inclination and displacement mode shape matrix. The proposed optimal sensor configuration can be used to select inclination-deflection transformation models that meet the required accuracy and stability from all possible sensor locations. In this study, the condition number and information entropy are employed to measure the ill-condition of the selected mode shape matrix and evaluate the prediction performance of different sensor configurations. The particle swarm optimization algorithm, genetic algorithm, and artificial fish swarm algorithm are used to optimize the sensor position placement. Numerical simulation and experimental validation results of a 5-span high-speed railway bridge show that the reconstructed deflection shapes agree well with those of the real bridge.

Keywords: high-speed railway bridge; dynamic deflection; optimal inclinometer sensor placement; inclination-deflection transformation; information entropy

1. Introduction

The dynamic deflection is widely considered as an important indicator for assessing the operational safety and structural damage of high-speed railway bridges. Hence, the dynamic deflection monitoring is also an important and indispensable part of Structural Health Monitoring (SHM) systems. In recent years, a large number of SHM systems have been implemented to obtain real-time structural information.

In the past decades, considerable efforts have been devoted to structural displacement reconstruction in the field of deformation monitoring. The strain measurement was employed to reconstruct the structural displacement based largely on the modal transformation method (Bogert *et al*. 2003, Foss and Haugse 1995). Pisoni *et al*. (1995) studied a beam structure with two strain gages and predicted the displacement at different locations of the beam. Li and Ulsoy (1999) studied the high-precision measurement of displacement for the precision flexible line boring using strain gages. The strain measured by the Fiber Bragg Grating (FBG) strain sensor can also be applied to the dynamical displacement reconstruction of structures based on the transformation matrix of the modal approach (Kim *et al*. 2011, Rapp *et al*. 2009, Kang *et al*. 2007, Zhou *et al*. 2019). Yang *et al*. (2017a) identified the full-field vibration modes of the structure from the video measurements, and then estimated the full-field dynamic strains based on the modal superposition method (Yang *et al*. 2019). In SHM systems of railway bridges, inclinometer sensors are usually employed for dynamic deflection monitoring. The traditional inclination-deflection principle is mostly based on mathematical theory, such as polynomial functions (Sousa *et al*. 2013), three spline interpolation principles (Xiong *et al*. 2018) and the combination of the orthogonal function and beam deflection constraint (He *et al*. 2014a, Hou *et al*. 2005). Shortcomings of these structural deflection reconstruction methods can be summarized as follows: (1) Most of the methods only consider the simple single-span beam structure. Although the relationship between deflection, strain, and modal shapes has theoretical solutions to a certain extent, the adopted approaches dealing with the ill-posed inverse problem are relatively simple; (2) With the increase of bridge spans, the undetermined parameters of the strain/inclination-deflection model increase dramatically. A large number of sensors are needed to meet the accuracy requirements of deflection prediction, which may result in a waste of material, labour, and financial resources. In addition, a large number of sensors can increase the occurrence of sensor anomalies, and the associated sensor maintenance may also be a major task for high-speed railway bridges; (3) The spatial correlation information hidden in strain/inclination measurements of different spans

*Corresponding author, Professor,
E-mail: lishunlong@hit.edu.cn

ISSN: 1738-1584 (Print), 1738-1991 (Online)

is ignored. Therefore, to satisfy the deflection prediction accuracy of the large complex high-speed railway bridges, it is necessary to propose a novel inclination-deflection model that accounts for the ill-posed inverse problem. In general, the prediction accuracy of the inclination-deflection model depends significantly on the placement of a limited number of inclinometer sensors for low cost and high efficiency. Thus, in order to obtain the most critical information with fewest inclinometer sensors, the installation positions of the inclinometer sensors need to be optimized to avoid the ill-conditioned modal matrix and improve the prediction accuracy.

In the field of modal updating and damage identification, the optimal sensor placement has been extensively studied and successfully applied in SHM systems (Azarbayejani *et al*. 2008, Flynn and Todd 2010, Heo *et al*. 1997, Li and Kiureghian 2016, Lu *et al*. 2016, Papadimitriou 2002, Papadimitriou *et al*. 2000, Trendafilova *et al*. 2001, Udwadia 1994, Lei *et al*. 2013, Pei *et al*. 2018, Yi *et al*. 2012). These include the effective independence sensor placement method (Kammer 1996), the kinetic energy method (Heo *et al*. 1997), the Bayesian-based framework method (Beck and Katafygiotis 1998), the information entropy-based method (Papadimitriou *et al*. 2000, Papadimitriou 2004), the intelligent optimization (Downey *et al*. 2018, Lian *et al*. 2013, Lin *et al*. 2018, Yang *et al*. 2017b, Yi *et al*. 2015, Zhou *et al*. 2015), etc. However, these optimal sensor placement methods are mainly focused on structural damage diagnosis and modal parameter identification. For displacement reconstruction and prediction, Zhang and Xu performed a sensor position optimization based on the principle of estimation error minimization (Zhang *et al*. 2011, 2014a). The optimal placement of FBG strain sensors also utilized the criteria of the conditional number minimization (Kim *et al*. 2011, Rapp *et al*. 2009), which required an exhaustive search to evaluate its performance for all sensor configurations to find the optimal solution. For the dynamical response reconstruction of structures, sequential sensor placement methods were proposed based on the state space equation (Hernandez 2017, Wang *et al*. 2014, Zhang and Xu 2016). The rank of Markov parameter matrix or the exhaustive search was usually employed to determine the initial sensor location. Then, one or multiple sensors were added at certain positions using a sequential placement algorithm based on the initial sensor locations (Wang *et al*. 2014, Zhang and Xu 2016). In this paper, for the large complex high-speed railway bridges with the degree of freedom over thousands, the inclinometer sensor is expected to capture all possible variable characteristics to provide more representative monitored dynamical deflections from thousands potential placement locations. Therefore, both data duplication and sensor expenses can be reduced by optimising reasonably the placement of the limited sensors.

In this study, the optimal inclinometer sensor placement for dynamic deflection monitoring in high-speed railway bridges is investigated to minimise the associated error of the proposed inclination-deflection transformation model. The paper is organized as follows: Section 2 illustrates the theoretical background and procedures of the proposed deflection monitoring method, including the development of the inclination-deflection transformation model, error analysis, and inclinometer sensor placement optimisation; Section 3 presents the numerical simulation and experimental verification of a typical high-speed railway bridge to assess the accuracy and robustness of the proposed model; finally, conclusions are drawn in Section 4.

2. Deflection monitoring using optimised inclinometer sensors

2.1 Inclination-deflection model establishment and prediction error analysis

Considering that the inclinometer sensor position is expressed as $d = [x, y, z]^T$, where *x*, *y* and *z* represent along-bridge, transverse-bridge, and vertical coordinates, respectively. The vertical displacement is often the main concern for the dynamic deflection monitoring of high-speed railway bridges, and can be expressed as

$$v(x,t) = \Phi(x)q(t) \tag{1}$$

where $v \in R^{N\times 1}$, $q \in R^{m\times 1}$ and $\Phi \in R^{N\times m}$ represent the deflection vector, generalized modal coordinates at time *t* and displacement mode shape matrix, respectively; N and m are the numbers of candidate inclinometer sensor locations and the selected modes. The vertical inclination of the measuring points for bending beam structures, as widely used in high-speed railway bridges, can be expressed as

$$\theta(x,t) = \frac{\partial v(x,t)}{\partial x} = \frac{d\,\Phi\,(x)}{d\,x} q(t) = \Psi(x)q(t) \tag{2}$$

where $\theta \in R^{M\times 1}$ and $\Psi \in R^{M\times m}$ indicate the vertical inclination vector at time *t* and candidate vertical inclination mode shapes, respectively.

Supposing that *M* inclinometer sensors are installed on high-speed railway bridges ($\theta \in R^{M\times 1}$ at time *t*), the inclination mode shape matrix $\Psi \in R^{M\times m}$ can be determined by the inclinometer sensor coordinates chosen from the *N* candidate inclinometer sensor locations ($M \ll N$). The generalized modal coordinate $\hat{q}_m$ can be solved using the Penrose-Moore generalized inverse as

$$\hat{q}(t) = \Psi^{+}(x)\theta(x,t) \tag{3}$$

where $\Psi^{+}(x) = [\Psi^T(x)\Psi(x)]^{-1}\Psi^T(x)$ if $\Psi \in R^{M\times m}$ is a column full rank matrix and $\Psi^{+}(x) = \Psi^T(x)[\Psi(x)\Psi^T(x)]^{-1}$ if $\Psi \in R^{M\times m}$ is a row full rank matrix. Once the generalized modal coordinates are obtained, the deflection at any section of the bridge can be expressed as

$$\hat{v}(x,t) = \Phi(x)\hat{q}(t) = \Phi(x)\Psi^{+}(x)\theta(x,t) \tag{4}$$

where $\hat{v} \in R^{P\times 1}$ and $\Phi \in R^{P\times m}$ indicate the reconstructed deflection vector and displacement mode shape matrix at

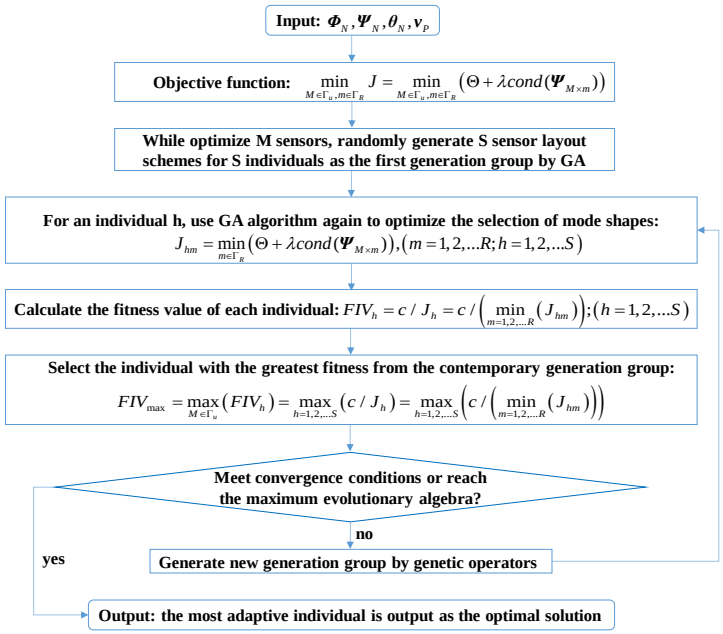

Fig. 1 Flow chart of the optimal placement of inclinometer sensors using the GA

the section P of the bridge. From Eq. (4), the deflection reconstruction $\hat{v}(x,t)$ accuracy can be significantly influenced by the Penrose-Moore generalized inverse $\Psi^+(x)$ and monitored inclination $\theta(x,t)$ errors.

The Penrose-Moore generalized inverse $\Psi^+(x)$ is uniquely determined by the degree of matrix morbidity of $\Psi \in R^{M\times m}$. This error represents the deviation between the expected deflection prediction and the true testing results, and accounts for the system error of the proposed inclination-deflection model. According to Eq. (4), the error caused by the Penrose-Moore generalized inverse $\Delta\Psi^+(x)$ can be expressed as

$$\delta_1(v) = \Phi(x)\Delta\Psi^+(x)\theta(x,t) \tag{5}$$

The monitored inclination $\hat{\theta}(x,t)$ is usually polluted with measurement noise$w$, and can be expressed as

$$\hat{\theta}(x,t) = \theta(x,t) + w \tag{6}$$

where w is assumed to be the zero-mean Gaussian noise with a variance of σ^2. The reconstruction error $\delta_2(v)$, which describes the testing error, is expressed as

$$\delta_2(v) = \Phi(x)\Psi^+(x)w \tag{7}$$

Combining Eqs. (4), (5) and (7), the total relative reconstruction error of deflection, when omitting high-order small quantities, can be expressed as

$$\delta(v) = \delta_1(v) + \delta_2(v) = \Phi(x)[\Delta\Psi^+(x)\theta(x,t) + \Psi^+(x)w] \tag{8}$$

2.2 Optimal inclinometer sensor placement and modal orders

From Eq. (8), both the system error and testing error of the proposed deflection prediction model depend mainly on the accuracy of the Penrose-Moore generalized inverse $\Psi^+(x)$, that is, the degree of matrix morbidity of $\Psi \in R^{M\times m}$. In this study, the row and column of the inclination mode shape matrix $\Psi \in R^{M\times m}$ are related to the selected inclinometer sensor coordinates and modal orders, which affect the accuracy and stability of the reconstructed deflection. The condition number is employed to measure the degree of matrix morbidity of $\Psi \in R^{M\times m}$. The reconstructed deflection is more accurate and stable when the condition number of Ψ becomes smaller. Therefore, the constructed smaller condition number matrix Ψ requires inclinometer sensor placement optimization and the condition number should be selected to obtain the objective function.

Furthermore, the information entropy (Papadimitriou *et al*. 2000, Papadimitriou 2004) was employed to measure the prediction accuracy of the inclination-deflection transformation model. According to Eq. (8), the reconstruction error of the deflection can be expressed as

$$\delta(v) = \delta_1(v) + \delta_2(v) = [\varepsilon^1;\cdots;\varepsilon^k;\varepsilon^P]^T \tag{9}$$

where the deflection error vector $\varepsilon^k(k = 1,2,\cdots,P)$ of the bridge section follows the Gaussian distribution with zero mean; and P represents the number of concerned sections. Therefore, the average information entropy Θ of deflection prediction errors can be expressed as

$$\Theta = \left(\sum_{k=1}^{P}\frac{1}{2}ln(2\pi e\hat{\sigma}_k^2)\right)/P \tag{10}$$

where $\hat{\sigma}_k^2$ is the variance estimation of the error vector $\varepsilon^k(k = 1,2,\ \cdots,P)$.

Taking into account the ill-posed inverse problem and

(a) The actual bridge

(b)

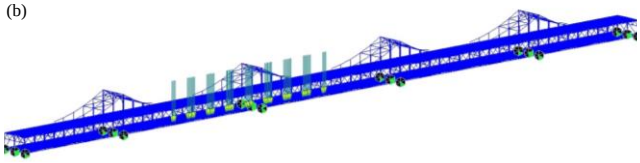

(b) The FEM with axle loads of the high-speed train

Fig. 2 5-span high-speed railway bridge

deflection prediction accuracy, the objective function for deflection prediction can be established as follows

$$\min_{M\in\Gamma_u, m\in\Gamma_R} J = \frac{1}{2P}\sum_{k=1}^{P} ln(2\pi e\hat{\sigma}_k^2) + \lambda cond(\Psi_{M\times m}) \quad (11)$$

where Γ_u denotes the set of candidate locations for installing the inclinometer sensors, Γ_R denotes the set of candidate modal orders and λ represents the adjustment coefficient between the condition number of Ψ_M and information entropy of the error matrix. λ should be properly selected to achieve a balance between the two sub-items for obtaining steady and reasonable solutions. Thus, the optimisation for deflection prediction accuracy aims to determine the sensor configuration with proper modal orders, corresponding to the minimum information entropy and condition number within all possible sensor locations and modal orders.

For the high-speed railway bridge with the set of candidate placement locations Γ_u and the set of mode shapes Γ_R, an exhaustive search for all potential sensor placements with corresponding mode shapes is quite time-consuming. In this study, the optimization problems, as shown in Eq. (11), can be solved by the Particle Swarm Optimization Algorithm (PSOA) (Lian *et al*. 2013, He *et al*. 2014b), Genetic Algorithm (GA) (Cha *et al*. 2012, He *et al*. 2013) and Artificial Fish Swarm Algorithm (AFSA) (Liu *et al*. 2019, Xu *et al*. 2019). All these algorithms are able to perform extensive searches on the global optimal sensor positions with the corresponding modal orders to prevent local optimal solutions. The flow chart of the optimal placement of inclinometer sensors using the GA is shown in Fig. 1.

Before performing sensor placement and modal optimization, it is important to select a proper number of mode shapes as the candidate set. In this paper, according to previous studies (Zhou *et al*. 2019, Zhang *et al*. 2014b), the Cumulative Effective Modal Mass Participation Ratio (CEMMPR) is used to determine the number of candidate mode shapes.

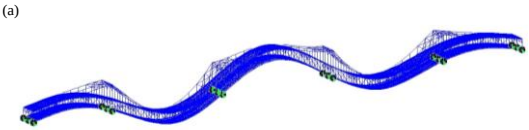

(a) The first mode shape

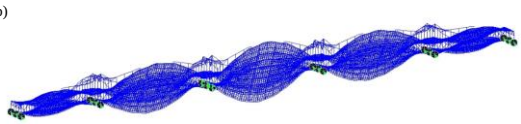

(b) The second mode shape

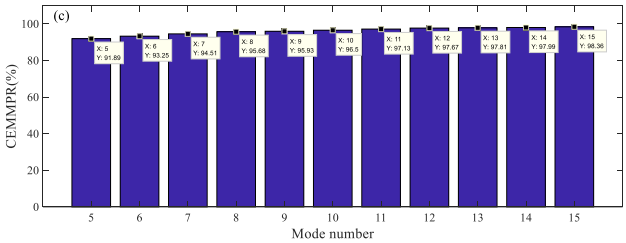

(c) The CEMMPR of the investigated bridge

Fig. 3 The first 2 mode shapes and the CEMMPR of the investigated bridge

3. Numerical simulation and experimental verification

3.1 5-span high-speed railway bridge

The investigated bridge in this study is a dual-use bridge with a four-lane railway lower deck and a six-lane highway upper deck, as shown in Fig. 2(a). The main bridge structure adopts a continuous steel truss beam with a total span of (128 + 3 × 180 + 128) m. The designed railway speeds for the passenger and freight lines are 250 km/h and 120 km/h, respectively. The designated health monitoring system of the bridge consists of the sensor subsystem, data acquisition and transmission subsystem, data processing and control subsystem, central database subsystem, early warning and analysis subsystem, and user interface subsystem. The general diagram and sensor layout of the SHM system are shown in Fig. 2(a). A total of 157 sensors were installed on the bridge to monitor the environmental and loading conditions, global responses, and local responses.

In this study, a three-dimensional (3D) Finite Element Model (FEM) of the investigated bridge was established using the software MIDAS/CIVIL 2017. In the FEM, the bridge deck was modelled by PLATE elements, the suspenders were modelled by TRUSS elements, and the other components were modelled by the cubic two-node BEAM elements. The bridge deck, main truss and transverse beams were connected by rigid connections. For the boundary conditions, the SJQZ spherical steel bearings at the 18 piers were simulated by fixed hinged supports that are capable of free rotation, unidirectional hinged supports that are capable of free rotation and transversal sliding, unidirectional hinged supports that are capable of free rotation and longitudinal sliding, bidirectional hinged supports that are capable of free rotation, transversal sliding

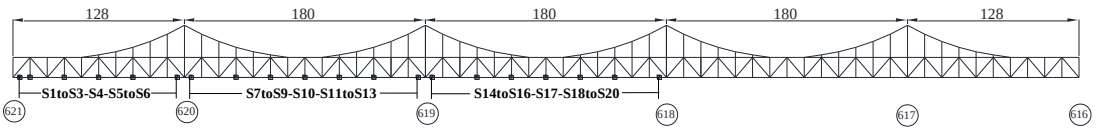

Schematic diagram of the installation position of 20 inclinometer sensors

Remarks:
1.Unit:m.
2.The ⑯, ⑰, ⑱, ⑲, ⑳, ㉑ represent the number of the pier.
3.The ▪ represent the installation position of 20 inclinometer sensors which are numbered S1 to S20 from left to right.

Fig. 4 Schematic of the positions of 20 inclinometer sensors on the bridge

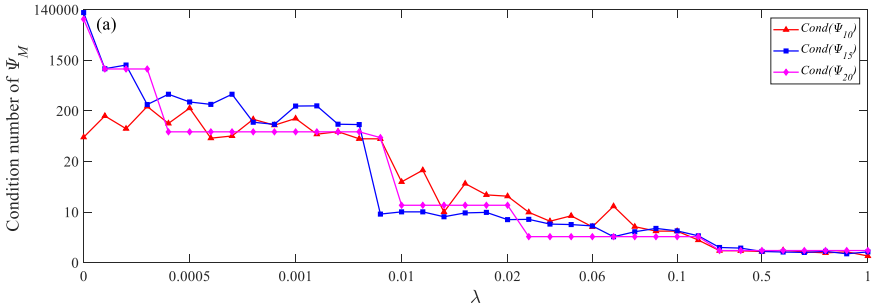

(a) The condition number of Ψ_M for different numbers of optimal sensors and λ

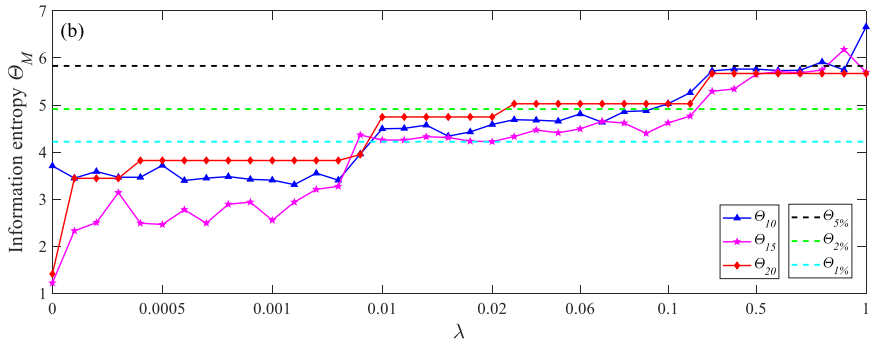

(b) The information entropy Θ_M for different numbers of optimal sensors and λ

Fig. 5 The condition number of Ψ_M and information entropy Θ_M for different numbers of optimal sensors and λ

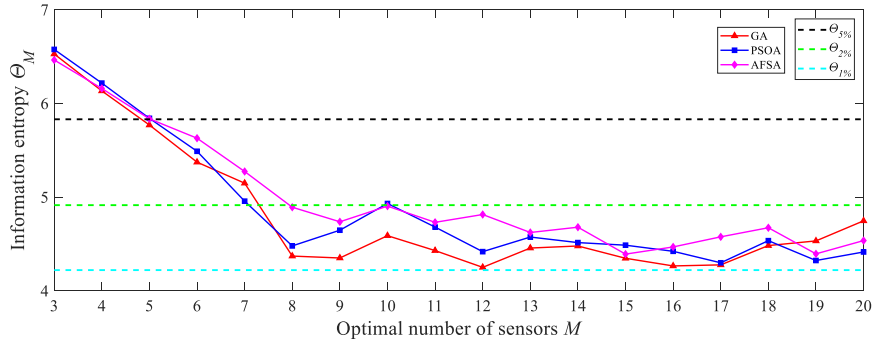

Fig. 6 Information entropy Θ_M with different numbers of optimal sensors using the three optimization algorithms

and longitudinal sliding, and their degrees of freedom were coupled in the simulation. In total, the FEM for the investigated bridge consists of 22673 BEAM elements, 96 TRUSS elements, and 12896 PLATE elements. Fig. 2(b) shows the established 3D FEM for the investigated bridge. Since the modal shape derived from FEM has certain influence on the accuracy of dynamical deflection monitoring, the FEM should be updated according to the collected data to incorporate more comprehensively the static and dynamic characteristics of the real bridge. In this paper, the response surface method (Goswami *et al*. 2016) was employed for finite element model updating. The comparison of the identified and analytical modal parameters, showing that the absolute relative differences of most of the frequencies are within 5%, which means that the updated FEM can simulate the dynamical behavior of

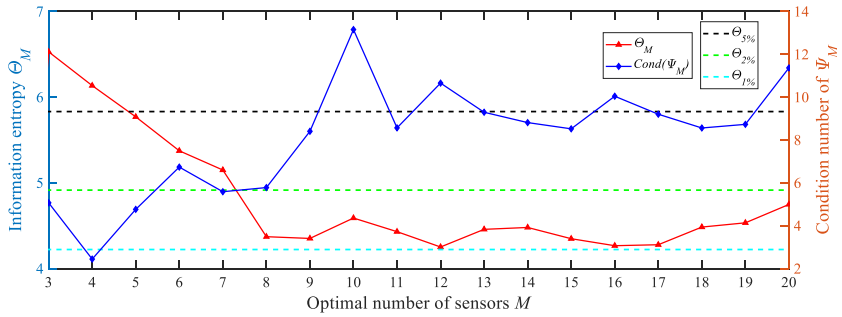

Fig. 7 The condition number of Ψ_M and information entropy Θ_M with different numbers of optimal sensors using the GA

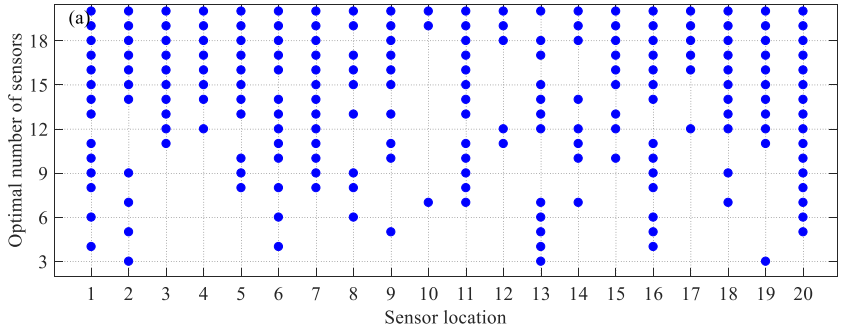

(a) The optimised sensor locations

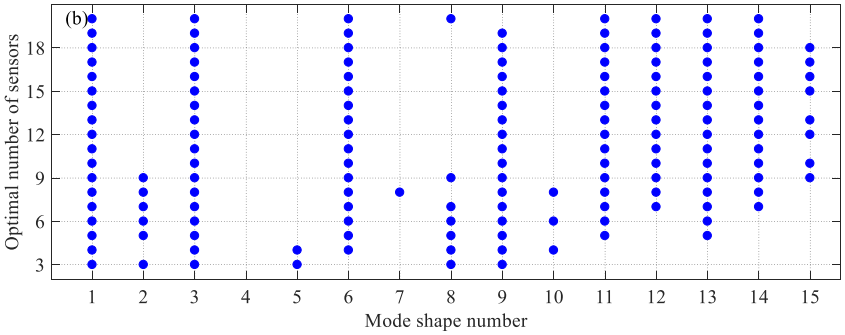

(b) The optimised mode shape number

Fig. 8 Optimization diagrams by the GA

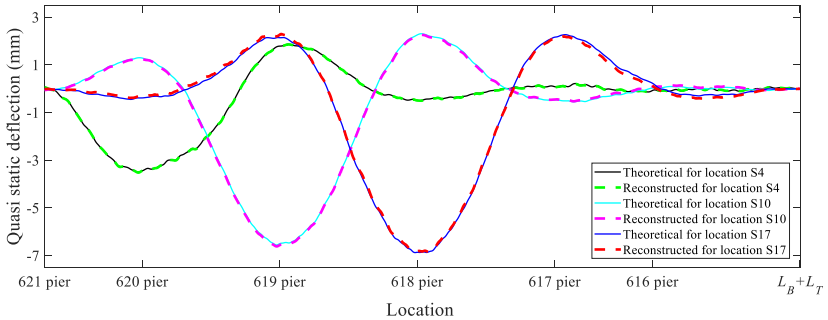

Fig. 9 Comparison of the theoretical and reconstructed quasi-static deflection for three key sections of the investigated bridge

actual bridge accurately to a certain extent.

3.2 Optimization of inclinometer sensor placement and modal orders

The row and column of the inclination mode shape matrix $\Psi \in R^{M\times m}$ are known to be related to the inclinometer sensor coordinates and modal orders. For the row of the matrix $\Psi \in R^{M\times m}$, 20 inclinometer sensors were permanently installed along the centreline of the railway bridge deck according to the experience of the engineers (as shown in Fig. 2(a)); while for the column of

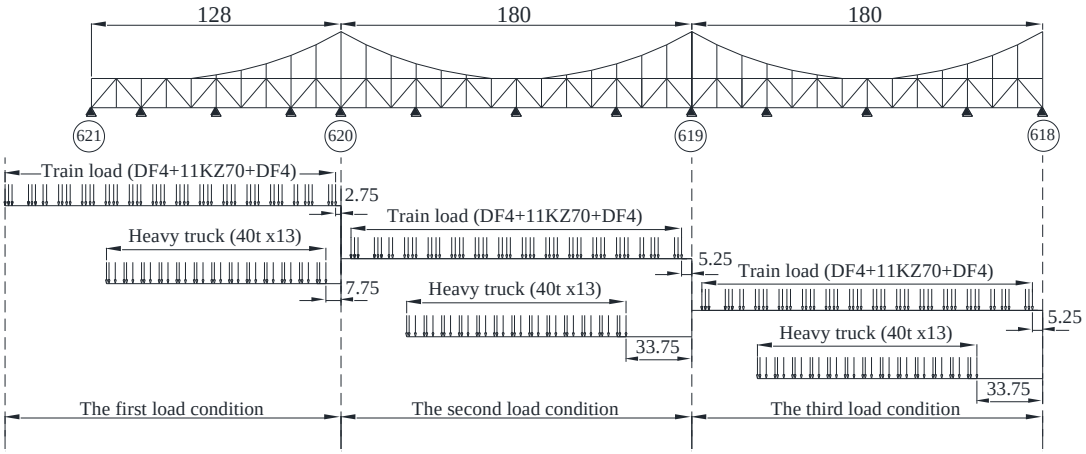

Remarks:
1.Unit:m.
2.The 618, 619, 620, 621 represent the number of the pier.
3.The ▲ represent the 13 measured points of the key sections.

Fig. 10 Schematic of the static loading test under three loading conditions (distance unit: m)

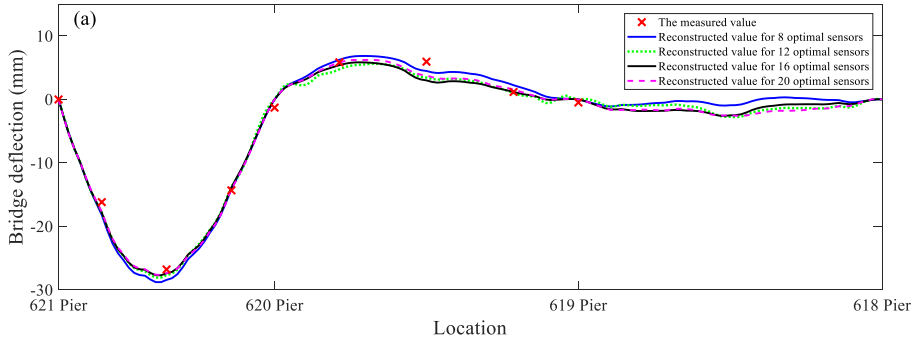

(a) The first loading condition

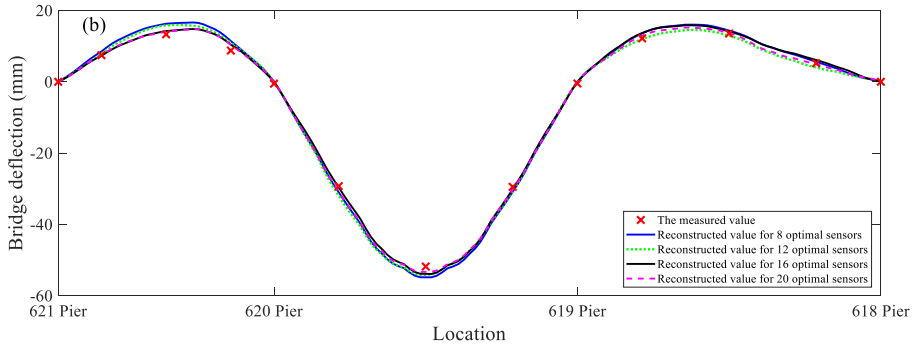

(b) The second loading condition

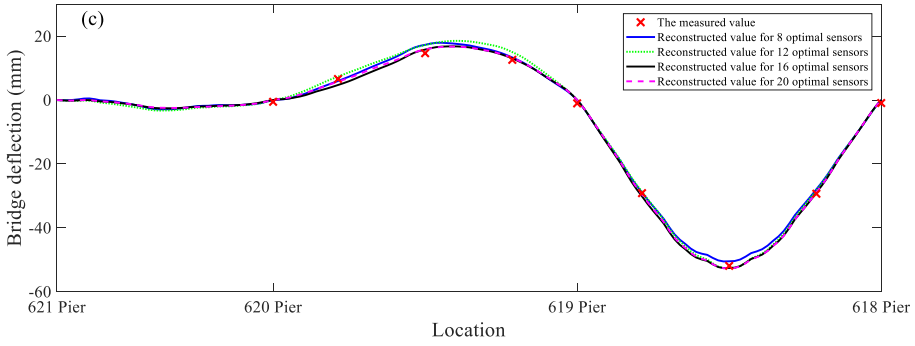

(c) The third loading condition

Fig. 11 Comparison between the reconstructed and measured bridge deflection

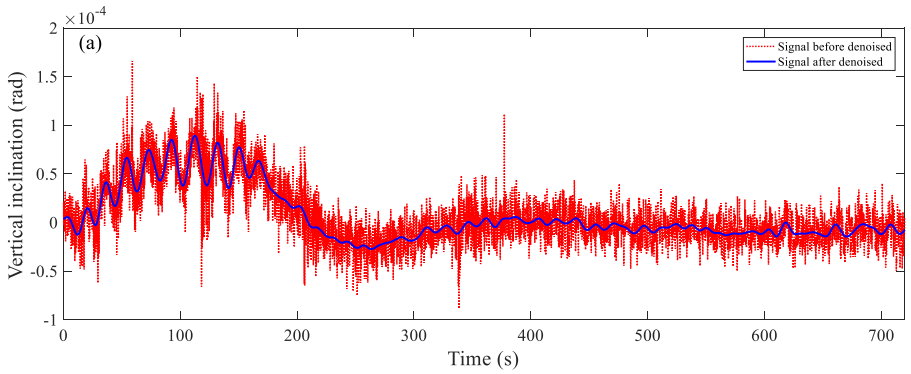

(a) The inclination of the sensor S2

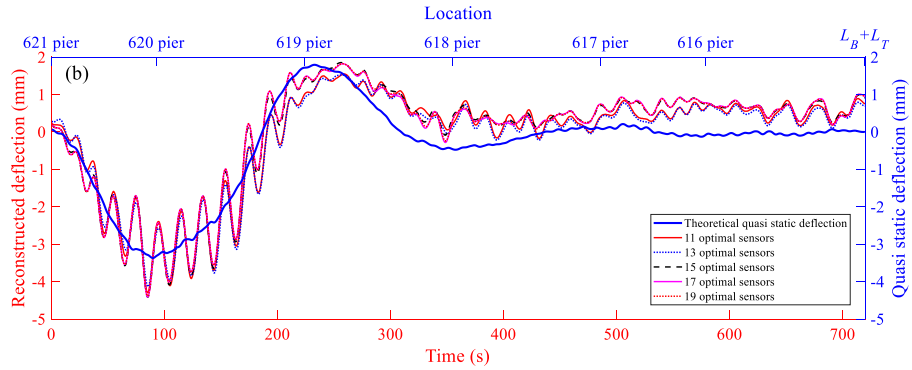

(b) The reconstructed bridge deflection at location S4

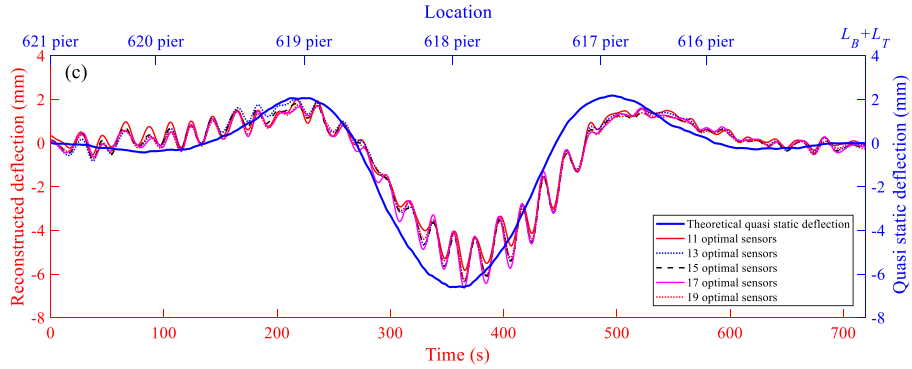

(c) The reconstructed bridge deflection at location S17

Fig. 12 Dynamic response of the bridge at a speed of 5 km/h

the matrix $\Psi \in R^{M\times m}$, the vertical and torsional modes were extracted using the updated FEM by Ritz vector methods. Since the deflection under train loads is the most important indicator in bridge assessment, the first 2 mode shapes and the CEMMPR were calculated as shown in Fig. 3. It can be seen from Fig. 3 that the CEMMPR of the first 5 and 15 modes of the investigated bridge was more than 90% and 98%, respectively (Zhou *et al*. 2019, Zhang *et al*. 2014b). However, the dynamical deflection monitoring of the investigated bridge showed that the deflection reconstruction (Eq. (4)) failed to achieve stable and acceptably accurate results using the 20 inclinations and 15 mode shapes and thus, they can be employed as candidates for accurate deflection reconstruction optimization.

In this study, the quasi-static inclination and deflection were generated by adding axle loads of a typical high-speed train to different locations of the updated FEM to simulate the train travelling at low speeds. The quasi-static inclination of 20 candidate nodes and the deflection of the concerned sections can be treated as measurements and objectives of deflection monitoring, respectively (as shown in Fig. 4).

Since the adjustment coefficient λ has great influence on the optimization results, the 10, 15 and 20 optimal inclination sensors with the corresponding modal orders were optimized with λ range from 0 to 1. The condition number of the inclination mode shape matrix $\Psi \in R^{M\times m}$ and the information entropy of the deflection error between the FEM and inclination calculated are shown in Fig. 5. It can be seen from Fig. 5 that the condition number decreases as the λ increases, while the information entropy shows the opposite trend. When λ is selected between 0.01 and 0.02, the condition number of Ψ_M is reduced to several tens and tends to be stabilized, with 2% of relative error for the information entropy. Thus, the adjustment coefficient λ was chosen at 0.02 in this study.

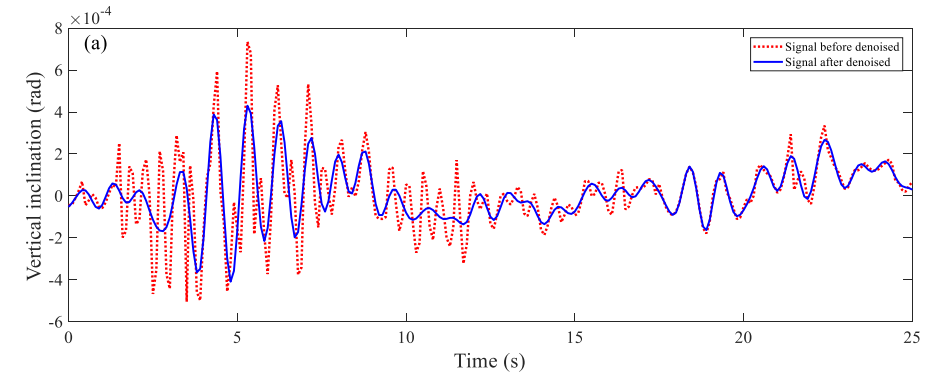

(a) The inclination of the sensor S2

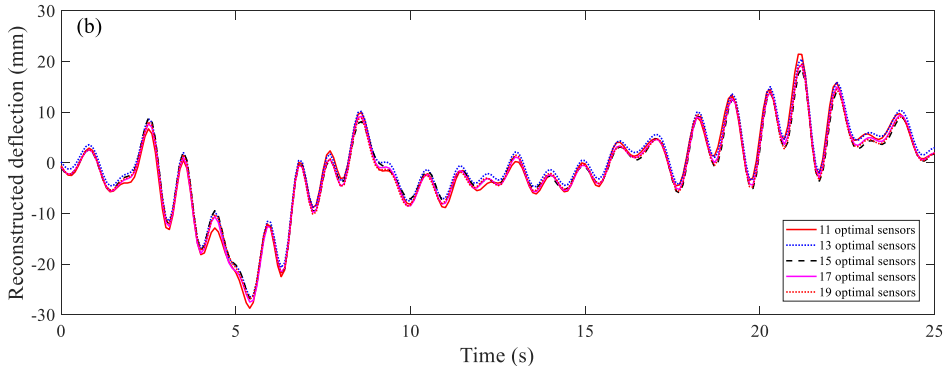

(b) The reconstructed bridge deflection at location S4

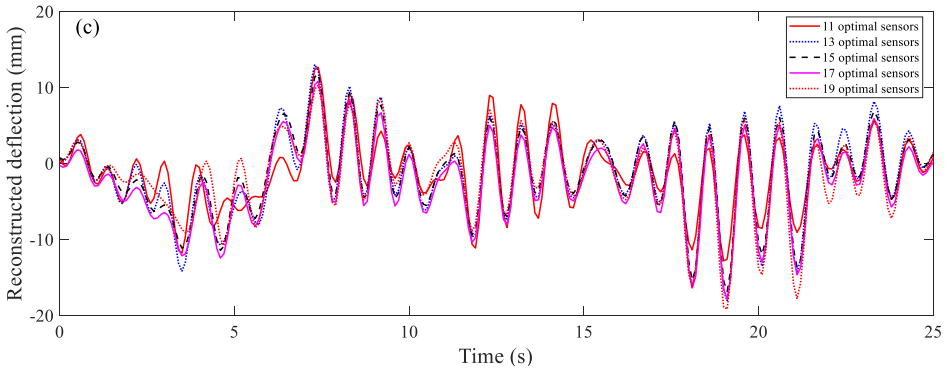

(c) The reconstructed bridge deflection at location S17

Fig. 13 Dynamic response of the bridge at a speed of 180 km/h

With the quasi-static inclination and the deflection extracted from the updated FEM, the PSOA, GA and AFSA were used to optimize the sensor location and the corresponding mode shapes orders. Fig. 6 illustrates the information entropy Θ_M for different numbers of optimal sensors. As can be observed from Fig. 6, the information entropy Θ_M decreases first and then becomes stabilized with the increase of sensor number. In general, the three optimization algorithms demonstrate nearly the same results. Compared with the PSOA and AFSA, the information entropy Θ_M from the GA is relatively low in most cases and thus, the GA was selected as the primary optimization algorithm in this study.

The information entropy Θ_M and condition number of Ψ_M are illustrated in Fig. 7 for different numbers of optimal sensors ranging from 3 to 20 using the GA algorithm. It can be seen from Fig. 7 that as the number of optimal sensors increases, the condition number of Ψ_M demonstrates some early fluctuations and then tends to become stabilized.

When the number of optimal inclinometer sensors is greater than 8, the information entropy Θ_M falls into a relative error level of 2% and remains stabilized. In addition, the condition number of Ψ_M is less than 14, showing that the ill-posed degree of matrix Ψ_M is well controlled.

The optimized sensor locations by the GA is shown in Fig. 8(a). It can be observed that the positions of the optimal sensors vary significantly as the sensor number increases, rather than a process of simply adding sensors over the original sensor configuration. The variation in the numbers of optimal sensor configurations can also reflect the spatial correlation information between each sensor, indicating that the optimized sensor configuration can represent the information contained in all sensors. The corresponding mode shape orders are shown in Fig. 8(b). As shown in the figure, some mode shapes are rarely or never

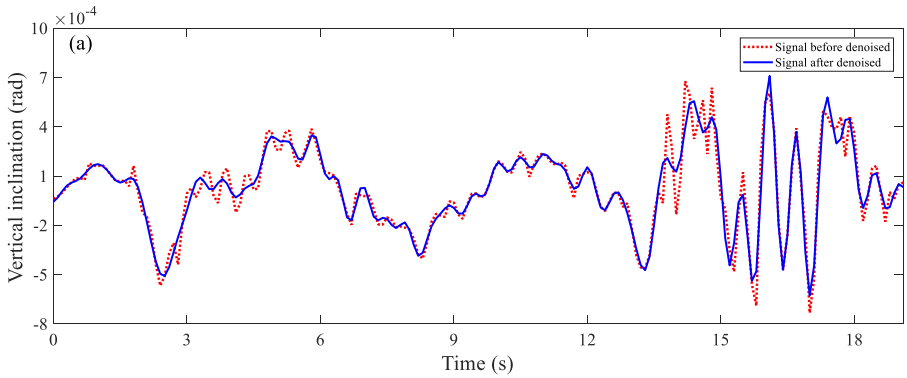

(a) The inclination of the sensor S2

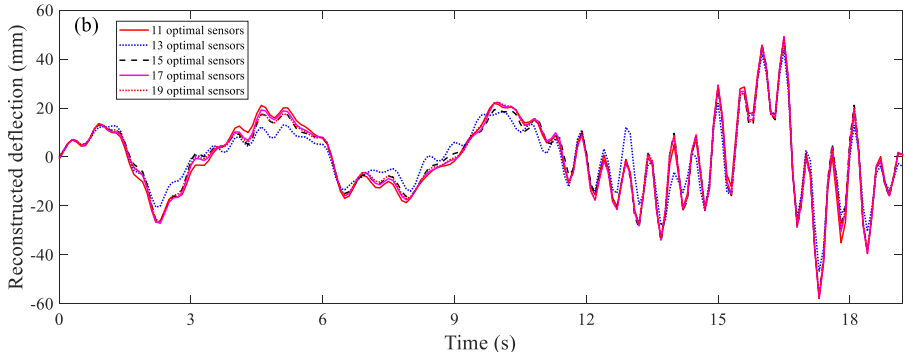

(b) The reconstructed bridge deflection at location S4

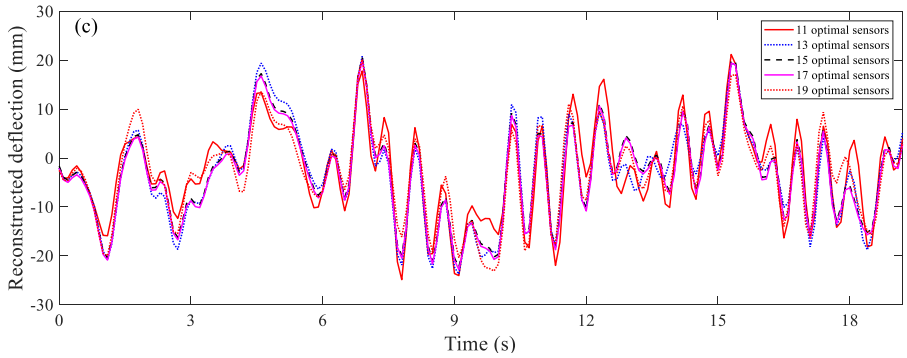

(c) The reconstructed bridge deflection at location S17

Fig. 14 Dynamic response of the bridge at a speed of 250 km/h

selected, such as the modes 4 and 7, this suggests that they can significantly increase the morbidity of the modal matrix Ψ_M.

Fig. 9 shows the comparison between the theoretical and reconstructed quasi-static deflection of three key sections of the investigated bridge using 8 optimal sensors by the GA. As illustrated in Fig. 9, the reconstructed deflection is generally identical to the theoretical result, showing that the optimal sensor locations with the corresponding orders can achieve an accurate and effective deflection monitoring. The 621 pier location on the *x*-coordinate represents where the first axle load of the high-speed train is introduced, whereas $L_T + L_B$ indicates where the last axle load of the high-speed train is removed.

3.3 Verification with static loading test

Prior to the official operation of a bridge, static and dynamic loading tests should be performed according to the design code requirements. Fig. 10 shows three loading conditions for the static loading test, including axle loads and loading positions. The train load DF4 + 11KZ70 + DF4 and load from 40 t × 13 heavy trucks were both applied to the railway line. During the test, the deflection of key sections was measured by the electronic total station system.

In this static loading test, the inclinations measured by different optimized inclinometer sensor numbers (i = 8, 12, 16, 20) can be used to predict the deflection of the key sections of the bridge. As can be seen from Fig. 11, under each loading condition, the reconstructed deflection of different numbers of optimal sensors agrees well with the measured values, showing that the inclination-deflection transformation model proposed in this paper is accurate and robust under the static loading condition.

3.4 Verification with dynamic loading test

After the completion of the 5-span high-speed railway bridge, the dynamic characteristics of the bridge was assessed to test the dynamic response of the test train when passing through the bridge at various speeds, to judge the working state of the bridge structure under dynamic loadings, to analyse and evaluate the stability of the test train passing through the bridge, and the dynamic performance of the bridge. The test train adopts the high-speed comprehensive inspection vehicle deployed by China Railway Corporation, and consists of 8 carriages in total. The speed grade test was carried out on October 14, 2018, by recording the bridge-head time and the bridge-tail time when the high-speed train passes the bridge during the dynamic load test. The bridge-head time represents the time when the train head reaches the bridge, whereas the bridge-tail time represents the time when the train tail leaves the bridge.

The three maximum speeds (unable to achieve absolute uniform speeds) of the train on the bridge were 5 km/h, 180 km/h, and 250 km/h, respectively. The sampling frequency of the inclinometers was 10 Hz. The measured inclinations were interspersed with many high-frequency signals (as shown in Fig. 12(a)) and the Butterworth low-pass filter was employed to retain the low-frequency signals, which correspond to the spatial distribution of the train wheelbase and the speed of the train when passing the bridge.

Figs. 12-14 show the comparison of the dynamic response of the bridge under different speeds. As shown in Fig. 12, when the speed of the train is 5 km/h, the inclination and reconstructed deflection variation can be obviously observed as each axle weight of the train passes the corresponding location. The 8 carriages of the test train can be simplified into 9 axle weights, which is consistent with the 9 peaks of the inclination and reconstructed deflection in Figs. 12(a)-(c). Moreover, the theoretical quasi-static deflection of the low-speed train was extracted from the FEM, showing close agreement with the trend of the reconstructed deflection. From Figs. 13 and 14, as the train speed increases, the impact force from the train increases accordingly, along with the increase of the predicted deflection. In addition, the predicted deflection has low volatility under different numbers of optimal sensor configurations, demonstrating the robustness of the proposed algorithm.

4. Conclusions

This paper provides a dynamic deflection monitoring method with the optimal inclinometer sensor placement for high-speed railway bridges. Based on the measured vertical inclinations from limited inclinometer sensors, the deflection shapes are reconstructed using a general inclination-deflection transformation. The following conclusions are obtained:

- A general inclination-deflection model is proposed and its prediction error is measured by the information entropy. By adjusting the condition number of the modal matrix to control the ill-conditioned degree, the genetic algorithm is used to optimize the sensor placement and selected mode shapes. The optimization results indicate that a sufficient number of sensors can be used to achieve an acceptable prediction accuracy for the proposed inclination-deflection model, and the ill-conditioned degree of the modal matrix can also be well controlled.
- The sensor placement schemes using three different optimization algorithms are discussed. Compared to the other two algorithms, the optimized sensor configuration scheme by the genetic algorithm shows the highest accuracy. When the number of sensors increases to a certain degree, the required prediction accuracy of the developed inclination-deflection model can be achieved and remains stabilized. The optimal sensor layout proposed in this study can improve the prediction accuracy of the inclination-deflection model, save the installation cost, and provide a reference for the maintenance of the inclinometer sensor. Results from the numerical simulation and experimental validation of the 5-span high-speed railway bridge show that the reconstructed shapes from the proposed method agree well with the real ones.

In traditional approaches, the number and location of inclinometer sensors often depend on the actual experience of the engineers. The optimal sensor placement method proposed in this paper can provide arrangements of the inclinometer in a more systematic and reasonable fashion. It also shows that the inclination-deflection model proposed in this paper can provide fundamental guidelines for the construction of the dynamic deflection monitoring system for high-speed railway bridges using the finite element numerical simulation.

Acknowledgments

Financial support for this study was provided by the National Key R&D Program of China [2018YFB1600200], NSFC [51922034, 51678204 and 51638007], Heilongjiang Natural Science Foundation for Excellent Young Scholars [YQ2019E025] and Guangxi Science Base and Talent Program [710281886032].

References

Azarbayejani, M., El-Osery, A.I., Choi, K.K. and Taha, M.M.R. (2008), "A probabilistic approach for optimal sensor allocation in structural health monitoring", *Smart Mater. Struct.*, **17**(5). https://doi.org/10.1088/0964-1726/17/5/055019.

Beck, J.L. and Katafygiotis, L.S. (1998), "Updating models and their uncertainties. I: Bayesian statistical framework", *J. Eng. Mech.*, **124**(4), 455-461. https://doi.org/10.1061/(ASCE)0733-9399(1998)124:4(455).

Bogert, P., Haugse, E. and Gehrki, R. (2003), "Structural shape identification from experimental strains using a modal transformation technique", *Proceedings of the 44th AIAA /ASME/ASCE/AHS/ASC Structures, Structural Dynamics and Materials Conference*, Virginia, USA, April.

Cha, Y.J., Agrawal, A.K., Kim, Y. and Raich, A.M. (2012), "Multi-objective genetic algorithms for cost-effective distributions of actuators and sensors in large structures", *Expert Syst. Appl.*,

39(9), 7822-7833. https://doi.org/10.1016/j.eswa.2012.01.070.
Downey, A., Hu, C. and Laflamme, S. (2018), "Optimal sensor placement within a hybrid dense sensor network using an adaptive genetic algorithm with learning gene pool", *Struct. Health Monit.*, **17**(3), 450-460. https://doi.org/10.1177/1475921717702537.
Flynn, E.B. and Todd, M.D. (2010), "A Bayesian approach to optimal sensor placement for structural health monitoring with application to active sensing", *Mech. Syst. Signal Process.*, **24**(4), 891-903. https://doi.org/10.1016/j.ymssp.2009.09.003.
Foss, G.C. and Haugse, E.D. (1995), "Using modal test results to develop strain to displacement transformations", *Proceedings of the 13th International Modal Analysis Conference*, Nashville, USA, February.
Goswami, S., Ghosh, S. and Chakraborty, S. (2016), "Reliability analysis of structures by iterative improved response surface method", *Struct. Safety.*, **60**, 56-66. https://doi.org/10.1016/j.strusafe.2016.02.002.
He, C., Xing, J.C., Li, J.L., Yang, Q.L., Wang, R.H. and Zhang, X. (2013), "A combined optimal sensor placement strategy for the structural health monitoring of bridge structures", *Int. J. Distrib. Sens. Netw.*, **9**(11), 820694. https://doi.org/10.1155/2013/820694.
He, L.J., Lian, J.J., Ma, B. and Wang, H.J. (2014a), "Optimal multiaxial sensor placement for modal identification of large structures", *Struct. Control Health Monit.*, **21**(1), 61-79. https://doi.org/10.1002/stc.1550.
He, X.L., Yang, X.S. and Zhao, L.Z. (2014b), "New method for high-speed railway bridge dynamic deflection measurement", *J. Bridge Eng.*, **19**(7), 05014004. https://doi.org/10.1061/(ASCE)BE.1943-5592.0000612.
Heo, G., Wang, M.L. and Satpathi, D. (1997), "Optimal transducer placement for health monitoring of long span bridge", *Soil Dyn. Earthq. Eng.*,**16**(7-8), 495-502. https://doi.org/10.1016/S0267-7261(97)00010-9.
Hernandez, E.M. (2017), "Efficient sensor placement for state estimation in structural dynamics", *Mech. Syst. Signal Process.*, **85**, 789-800. https://doi.org/10.1016/j.ymssp.2016.09.005.
Hou, X.M., Yang, X.S. and Huang, Q. (2005), "Using inclinometers to measure bridge deflection", *J. Bridge Eng.*, **10**(5), 564-569. https://doi.org/10.1061/(ASCE)1084-0702(2005)10:5(564).
Kammer, D.C. (1996), "Optimal sensor placement for modal identification using system-realization methods", *J. Guid. Control Dyn.*, **19**(3), 729-731. https://doi.org/10.2514/3.21688.
Kang, L.H., Kim, D.K. and Han, J.H. (2007), "Estimation of dynamic structural displacements using fiber Bragg grating strain sensors", *J. Sound Vib.*, **305**(3), 534-542. https://doi.org/10.1016/j.jsv.2007.04.037.
Kim, H.I., Kang, L H. and Han, J.H. (2011), "Shape estimation with distributed fiber Bragg grating sensors for rotating structures", *Smart Mater. Struct.*, **20**(3), 035011. https://doi.org/10.1088/0964-1726/20/3/035011.
Lei, Y., Liu, C., Jiang, Y.Q. and Mao, Y.K. (2013), "Substructure based structural damage detection with limited input and output measurements", *Smart Struct. Syst., Int. J.*, **12**(6), 619-640. http://dx.doi.org/10.12989/sss.2013.12.6.619.
Li, B.B. and Kiureghian, A.D. (2016), "Robust optimal sensor placement for operational modal analysis based on maximum expected utility", *Mech. Syst. Signal Process.*, **75**, 155-175. https://doi.org/10.1016/j.ymssp.2016.01.005.
Li, C.J. and Ulsoy, A.G. (1999), "High-precision measurement of tool-tip displacement using strain gauges in precision flexible line boring", *Mech. Syst. Signal Process.*, **13**(4), 531-546. https://doi.org/10.1006/mssp.1999.1223.
Lian, J.J., He, L.J., Ma, B., Li, H.K. and Peng, W.X. (2013), "Optimal sensor placement for large structures using the nearest neighbour index and a hybrid swarm intelligence algorithm", *Smart Mater. Struct.*, **22**(9), 095015. https://doi.org/10.1088/0964-1726/22/9/095015.
Lin, J.F., Xu, Y.L. and Law, S.S. (2018), "Structural damage detection-oriented multi-type sensor placement with multi-objective optimization", *J. Sound Vib.*, **422**, 568-589. https://doi.org/10.1016/j.jsv.2018.01.047.
Liu, Y., Tao, Z.P., Yang, J. and Mao, F. (2019), "The modified artificial fish swarm algorithm for least-cost planning of a regional water supply network problem", *Sustainability*, **11**(15), 4121. https://doi.org/10.3390/su11154121.
Lu, W., Wen, R.F., Teng, J., Li, X.L. and Li, C. (2016), "Data correlation analysis for optimal sensor placement using a bond energy algorithm", *Measurement*, **91**, 509-518. https://doi.org/10.1016/j.measurement.2016.05.089.
Papadimitriou, C. (2002), "Applications of genetic algorithms in structural health monitoring", *Proceedings of the 5th World Congress on Computational Mechanics*, Vienna, Austria, August.
Papadimitriou, C. (2004), "Optimal sensor placement methodology for parametric identification of structural systems", *J. Sound Vib.*, **278**(4-5), 923-947. https://doi.org/10.1016/j.jsv.2003.10.063.
Papadimitriou, C., Beck, J.L. and Au, S.K. (2000), "Entropy-based optimal sensor location for structural model updating", *J. Vib. Control.*, **6**(5), 781-800. https://doi.org/10.1177/107754630000600508.
Pei, X.Y., Yi, T.H. and Li, H.N. (2018), "A multitype sensor placement method for the modal estimation of structure", *Smart Struct. Syst., Int. J.*, **21**(4), 407-420. http://dx.doi.org/10.12989/sss.2018.21.4.407.
Pisoni, A.C., Santolini, C., Hauf, D.E. and Dubowsky, S. (1995), "Displacements in a vibrating body by strain gage measurements", *Proceedings of the SPIE the International Society for Optical Engineering*, Fano, Italy, July.
Rapp, S., Kang, L.H., Han, J.H., Mueller, U.C. and Baier, H. (2009), "Displacement field estimation for a two-dimensional structure using fiber Bragg grating sensors", *Smart Mater. Struct.*, **18**(2), 025006. https://doi.org/10.1088/0964-1726/18/2/025006.
Sousa, H., Cavadas, F., Henriques, A., Bento, J. and Figueiras, J. (2013), "Bridge deflection evaluation using strain and rotation measurements", *Smart Struct. Syst., Int. J.*, **11**(4), 365-386. http://dx.doi.org/10.12989/sss.2013.11.4.365.
Trendafilova, I., Heylen, W. and Van Brussel, H. (2001), "Measurement point selection in damage detection using the mutual information concept", *Smart Mater. Struct.*, **10**(3), 528-533. https://doi.org/10.1088/0964-1726/10/3/315.
Udwadia, F.E. (1994), "Methodology for optimum sensor locations for parameter-identification in dynamic-systems", *J. Eng. Mech.*, **120**(2), 368-390. https://doi.org/10.1061/(ASCE)0733-9399(1994)120:2(368).
Wang, J., Law, S.S. and Yang, Q.S. (2014), "Sensor placement method for dynamic response reconstruction", *J. Sound Vib.*, **333**(9), 2469-2482. https://doi.org/10.1016/j.jsv.2013.12.014.
Xiong, H.B., Cao, J.X. and Zhang, F.L. (2018), "Inclinometer-based method to monitor displacement of high-rise buildings", *Struct. Monit. Maint., Int. J.*, **5**(1), 111-127. https://doi.org/10.12989/smm.2018.5.1.111.
Xu, H., Zhao, Y.Q., Ye, C. and Lin, F. (2019), "Integrated optimization for mechanical elastic wheel and suspension based on an improved artificial fish swarm algorithm", *Adv. Eng. Softw.*, **137**, 102722. https://doi.org/10.1016/j.advengsoft.2019.102722.
Yang, C., Zhang, X.P., Huang, X.Q., Cheng, Z.A., Zhang, X.H. and Hou, X.B. (2017a), "Optimal sensor placement for deployable antenna module health monitoring in SSPS using

genetic algorithm", *Acta Astronaut*., **140**, 213-224. https://doi.org/10.1016/j.actaastro.2017.08.025.

Yang, Y., Dorn, C., Mancini, T., Talken, Z., Kenyon, G., Farrar, C. and Mascarenas, D. (2017b), "Blind identification of full-field vibration modes from video measurements with phase-based video motion magnification", *Mech. Syst. Signal Process*., **85**, 567-590. https://doi.org/10.1016/j.ymssp.2016.08.041.

Yang, Y., Jung, H.K., Dorn, C., Park, G., Farrar, C. and Mascareñas, D. (2019), "Estimation of full-field dynamic strains from digital video measurements of output-only beam structures by video motion processing and modal superposition", *Struct. Control Health Monit*., **26**(10), 2408. https://doi.org/10.1002/stc.2408.

Yi, T.H., Li, H.N. and Gu, M. (2012), "Sensor placement for structural health monitoring of Canton tower", *Smart Struct. Syst*., *Int. J*., **10**(4-5), 313-329. https://doi.org/10.12989/sss.2012.10.4_5.313.

Yi, T.H., Li, H.N. and Zhang, X.D. (2015), "Sensor placement optimization in structural health monitoring using distributed monkey algorithm", *Smart Struct. Syst., Int. J*., **15**(1), 191-207. https://doi.org/10.12989/sss.2015.15.1.191.

Zhang, C.D. and Xu, Y.L. (2016), "Optimal multi-type sensor placement for response and excitation reconstruction", *J. Sound Vib*., **360**, 112-128. https://doi.org/10.1016/j.jsv.2015.09.018.

Zhang, X.H., Zhu, S., Xu, Y.L. and Homg, X.J. (2011), "Integrated optimal placement of displacement transducers and strain gauges for better estimation of structural response", *Int. J. Struct. Stab. Dyn*., **11**(3), 581-602. https://doi.org/10.1142/S0219455411004221.

Zhang, X.H., Xu, Y.L., Zhu, S.Y. and Zhan, S. (2014a), "Dual-type sensor placement for multi-scale response reconstruction", *Mechatronics*, **24**(4), 376-384. https://doi.org/10.1016/j.mechatronics.2013.05.007.

Zhang, X., Li, J.L., Xing, J.C., Wang, P., Yang, Q.L., Wang, R.H. and He, C. (2014b), "Optimal sensor placement for latticed shell structure based on an improved particle swarm optimization algorithm", *Math. Probl. Eng*., **2014**, 1-12. https://doi.org/10.1155/2014/743904.

Zhou, G.D., Yi, T.H., Zhang, H. and Li, H.N. (2015), "Optimal sensor placement under uncertainties using a nondirective movement glowworm swarm optimization algorithm", *Smart Struct. Syst*., *Int. J*., **16**(2), 243-262. https://doi.org/10.12989/sss.2015.16.2.243.

Zhou, J.Z., Cai, Z., Kang, L., Tang, B.F. and Xu, W.H. (2019), "Deformation sensing and electrical compensation of smart skin antenna structure with optimal fiber Bragg grating strain sensor placements", *Compos. Struct*., **211**, 418-432. https://doi.org/10.1016/j.compstruct.2018.12.048.